

6 Search for SIMPs using Trackless Jets

The monojet dark matter search detailed in Chapter 5 can be complemented at high interaction cross sections by a different search which does not look for dark matter in the form of missing transverse momentum. Indeed, if the dark matter particles have an interaction cross section of the order of the strong interaction, they will interact in the detector, mainly in the calorimeters. The analysis described in this chapter is based on this scenario, and the considered simplified model is specified in Section 2.3.1. In this model, the dark matter particles are produced in pairs through a new strongly interacting mediator, and give rise to a pair of trackless jets as signature. Since the produced strongly interacting massive particles (SIMPs) are neutral, the resulting jets can be distinguished from QCD jets using the jet charged hadron energy fraction (CHF). The signal region where the SIMPs are being looked for is therefore defined by requiring the two leading jets to have a low CHF. In the control region, which is used to predict and validate the expected background, one or both jets are required to have a large CHF.

Firstly, the applied jet and photon reconstruction and identification are described, as well as the specific treatment applied for the primary vertex selection. The triggers that were designed specifically for this search, exploiting the CHF, are outlined in Section 6.2. However, these triggers were found to be problematic and eventually a generic single jet trigger was used instead. Next, the event selection is detailed in Section 6.3 for both the signal and control regions. The strategy for the background estimation and the systematic uncertainties are discussed in Sections 6.4 and 6.5, respectively. Finally, in Sections 6.6 and 6.7, the results are shown and interpreted in terms of the SIMP simplified model described in Section 2.3.

6.1 Physics object reconstruction

In this analysis, jets with a very small charged hadron energy fraction (CHF) are being searched for. Since these are rather peculiar jets containing no or very few tracks, a good primary vertex selection and photon identification play an important role in suppressing the main physics and reconstruction backgrounds.

6.1.1 Jets

For the jet reconstruction, the standard method described in Section 4.3.7 is used. Although the jets in the signal samples are expected to be neutral, it is beneficial to use PF jets because they directly provide an unambiguous association of tracks to jets. The standard jet energy corrections are applied as well, while the standard jet identification criteria are not used, since several of the quality criteria would actually remove the neutral SIMP jets.

6.1.2 Photons

Since photons might be reconstructed as neutral jets, photon + jets events are an important background for the control as well as the signal region. The photons therefore need to be identified and rejected, which is done using the standard photon loose identification described in Section 4.3.3. Further photon rejection is achieved by analysis-specific selections on photon conversions and on the jet neutral electromagnetic energy fraction (NEMF), as described in Section 6.3.

6.1.3 Primary vertex

The standard primary vertex reconstruction described in Section 4.3.1 sometimes provides a wrong primary vertex, which arises from a pileup interaction. The choice of a wrong vertex is not a problem in the case of signal events, which will pass in particular the CHF cuts in the event selection detailed in Section 6.3 just as easily. However, a wrongly chosen vertex in a QCD background event leads to the jets having an artificially very low CHF, both in simulation and data, as the standard charged hadron subtraction (CHS) procedure will remove the tracks from the vertex of the true hard interaction. This makes such events appear signal-like. For the lowest jet charged hadron energy fractions considered in this analysis, this background of events with a misidentified primary vertex becomes dominant with respect to the background from QCD events with a very rare jet fragmentation into predominantly neutral hadrons and photons. In Figure 6.1 an event display is shown that demonstrates such a wrong choice of vertex.

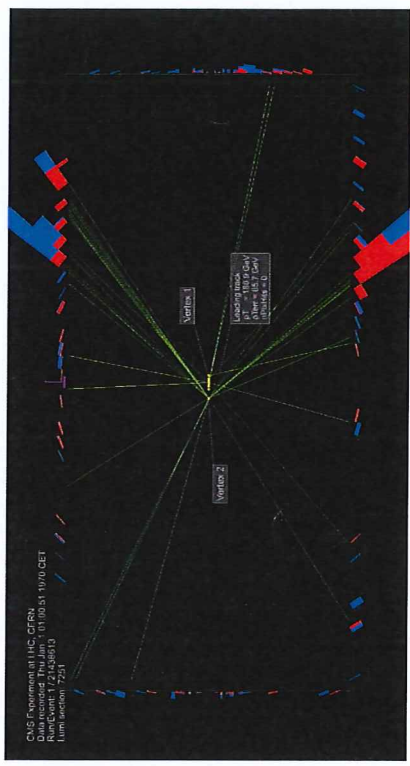


Figure 6.1: Event display showing an example of a wrong primary vertex selection in a MC-simulated QCD event. Although "Vertex 1" is the real vertex of the hard collision, "Vertex 2" is selected because of the presence of a single high- p_T track with poor momentum resolution and no pixel hits attached. As a result, the two visible high- p_T jets (above 200 GeV), clearly with many tracks attached, are reconstructed with only 3% and 4% of charged energy fraction.

Investigating this problem, many events with a wrong vertex assignment were observed to have the highest- p_T track being of poor quality, with a high momentum with large uncertainty, and no pixel hits. This alone, though, does not provide a sufficient handle to suppress this background, and a plain cut on number of pixel hits was verified to remove a lot of signal events as well. Studying the simulated misidentification by analysing event displays also showed that the true vertex is reconstructed as the second vertex in the list for the far majority of the cases. A second jet reconstruction was therefore produced, based on selecting the second entry in the list of primary vertices to be the event's collision vertex, and rerunning the CHS as well. If this second vertex was the correct one, the jets will now have a large CHF in most of the cases, while the first event reconstruction yields low-CHF jets. In the event

*discuss signal efficiency of
M and photon bkg mode*

6.3 Event selection

The event selection aims to select back-to-back dijet events with a low CHF. As a baseline selection, the two highest- p_T jets are required to have $p_T > 550$ GeV, in order to ensure the jets to be above the turn-on of the trigger. Furthermore, they are required to have $|\eta| < 2.0$, placing them fully within the tracking volume, thus suppressing backgrounds from jets that have a low CHF due to tracks falling out of tracker acceptance. Since the SIMPs do not undergo parton showering, while QCD partons undergo final state radiation, events with SIMPs have a lower number of jets than QCD multijet events, as can be seen from the top right plot in Figure 6.5. Events containing additional jets with $p_T > 30$ GeV in the full η acceptance of the CMS calorimeters on top of the two leading jets are therefore vetoed.

A photon veto is also applied to suppress photon + jets events. This is done by rejecting events with a photon within $\Delta R < 0.1$ of the leading or subleading jet, using the loose working point of the cut-based photon identification to identify photons, as described in Section 4.3.3. In some cases, however, jets have a large photon energy fraction, but the photon in the jet does not pass the loose identification requirements, for instance when there is a photon conversion in the tracker. In order to reject photon + jets events more efficiently, an additional cut is applied, as described in Section 4.3.3.

In order to avoid any problems related to the striking discrepancy in the top left plot of Figure 6.5, at least two reconstructed vertices are required. Additionally, the azimuthal separation of the two selected jets is required to be $\Delta\phi > 2$. Finally, noise filters are applied in order to reject beam halo or instrumental background, such as noise in the calorimeters.

Table 6.2 shows the number of events remaining in data, for simulated QCD events, and for 2 signal samples, after consecutively applying the described selection cuts. This shows that the background is already reduced by a factor 5, mainly by the cut on the number of jets, while a high efficiency is maintained for the signal. In Figure 6.6, data, QCD multijet simulation, and signal are compared after these selections, for the p_T , η and CHF of the two leading jets. Figure 6.5 shows the distribution of the number of vertices, the number of jets, $\Delta\phi(\text{jet1}, \text{jet2})$, and H_T , which is defined as the sum of the transverse momenta of the two jets. In some cases, all the selection cuts except the cut on the variable being shown are applied. The bump and long tail that can be seen in the data for the $\Delta\phi(\text{jet1}, \text{jet2})$ distribution contain events coming from processes with a heavy vector boson, such as Z + jets or W + jets, or $t\bar{t}$ events. The simulation instead shows a steeply falling spectrum since only QCD dijet events are shown. Contributions from Z + jets or W + jets, and $t\bar{t}$ events were verified to be negligible in the signal region using simulated samples.

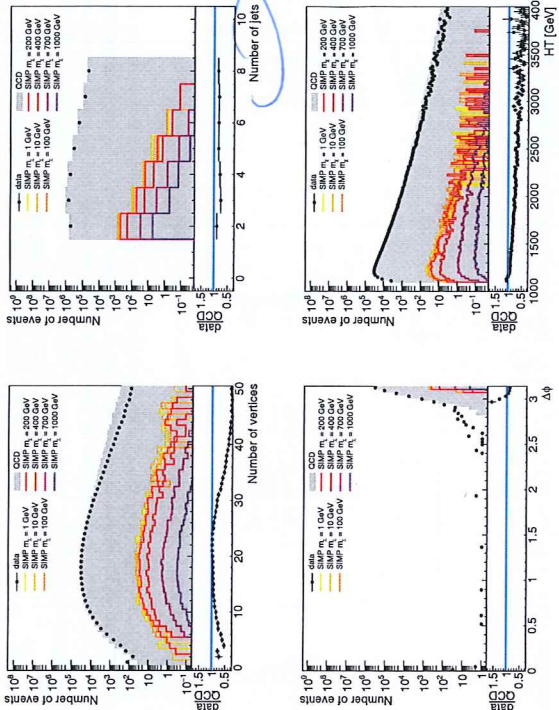


Figure 6.5: Number of vertices, number of jets, $\Delta\phi(\text{jet1}, \text{jet2})$, and H_T distributions, with selection cuts applied. The requirement on the number of vertices is not applied for the corresponding plot, the cut on the number of jets is not applied for the number of jets distribution, and the $\Delta\phi$ cut is similarly not applied for the corresponding distribution.

1 signal cut being considered. In this case, the cut is applied for both reconstructions starting from the first
2 and second primary vertex.

6.4 Background estimation

4 The main background for this analysis are QCD multijets. This background is estimated from data, as
5 the simulation does not describe the data well, especially at low CHF. The signal events can then be
6 distinguished from this background using the jet CHF. A second background comes from photon + jets
7 events. However, this background is efficiently removed by applying a photon veto.

6.4.1 Photon + jets

9 The photon + jets background was studied using a high- H_T MC sample generated at LO with MAD-
10 GRAPH5@NLO, hadronized with PYTHIA 8, and simulated and reconstructed using the standard
11 procedure described in Chapter 4. The used sample corresponds to about $275b^{-1}$, which is larger than
12 the data sample used for this analysis and is therefore sufficient to evaluate its contribution in the signal
13 region. This background is verified to be negligible after applying the signal region event selection, and
14 well within any other systematic uncertainty on the background prediction. The photon veto works well,
15 especially the cut on the jet neutral electromagnetic fraction, and no events from the used simulated pho-
16 ton + jets sample remain after applying a cut of $\text{CHF} < 0.1$. Additionally, in part of the events remaining
17 just above that cut the photon is not identified because it is very close to a jet. These events are therefore
18 already contained in the overlapping QCD multijets sample.

Table 6.2: Number of events remaining after the listed selection cuts in data, QCD events, and *#* 2 signal samples.

selection cut		yield		
	data	QCD MC	SIMP ($m_\chi = 1000$ GeV)	SIMP ($m_\chi = 1000$ GeV)
$p_T^{j1,j2} > 550$ GeV	2540420	3152550	773	5.7
$ \eta_{j1,j2} < 2.0$	2441240	2989320	748	5.6
# jets = 2	534053	587670	636	4.9
photon veto	531366	586674	636	4.9
# vertices ≥ 2	531244	586641	636	4.9
$\Delta\phi(j1, j2) > 2$	531207	586641	636	4.9
noise filters	528614	5821184	634	4.9

33 As will be detailed in Section 6.4, the background is predicted from a data control region where at least
34 one of the leading jets has a high CHF, above 0.25. No further selection on the second reconstruction with
35 respect to the second primary vertex is applied for the control region, since the presence of at least one
36 jet with a large CHF avoids the problem of the wrong selection of primary vertex detailed in Section 6.1.
37 In the case of the signal region selection, both jets are required to have $\text{CHF} < x$, where x is the

*Muon+... found to be sufficient! is soft
photon*

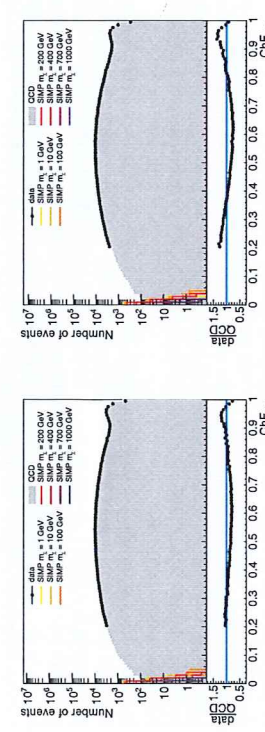
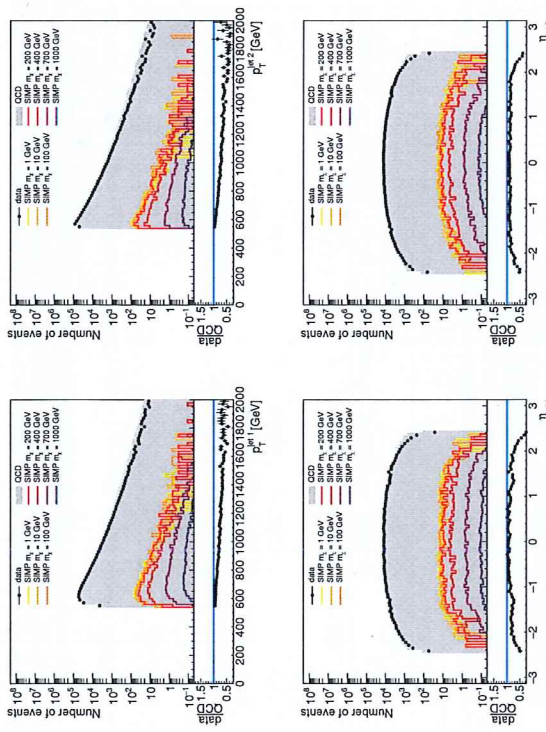


Figure 6.6: p_T , η , and CHF of the leading (left) and subleading (right) jet. The selection cuts are applied, except for the cut on η in the corresponding plot.

6.4.2 QCD multijets

The QCD multijet background is estimated from data, since the simulation does not describe the data well, especially at low CHF, as can be seen from Figure 6.7 which compares the CHF distribution in the control region to the QCD MC. In this plot the subleading jet is required to have a large CHF, in order to stay in the control region.

As a first step, the efficiency of the CHF cut is measured in the control region, by tagging one jet with high CHF and applying the CHF cut on the other jet. The efficiency is then given by the ratio of the number of events passing the cut divided by the total number of events selected in the control region. The measurement is performed in bins of jet p_T and η . The number of QCD events in the signal region is then predicted by using any QCD dijet event passing the selection cuts listed in Table 6.2 and applying the appropriate p_T and η dependent CHF cut efficiencies on the two leading jets. Figure 6.8 shows the

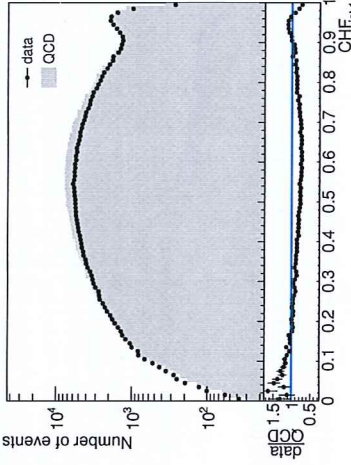


Figure 6.7: Data-MC comparison of the charged energy fraction of the leading jet, tagging events with subleading jet $CHF > 0.5$.

measured 1D efficiency as a function of the CHF cut for various bins in p_T^{jet} and η_{jet} , as measured in the QCD MC. There is a strong dependence on the jet p_T , and a less pronounced dependence on the jet η at low CHF. The efficiencies are the highest for the $1.0 < |\eta| < 1.25$ bin, which can be attributed to this being the barrel-endcap transition region where most of the tracker material is located. The dependence on the jet p_T arises from the reconstruction. As can be seen from the left plot in Figure 6.9, at generator level the CHF is independent of the jet p_T , as one would expect. After reconstruction, as demonstrated in the right plot of Figure 6.9, a p_T dependence arises due to the known degradation of tracking efficiency in dense jet environments, which becomes more of an issue for very high p_T and thus collimated jets.

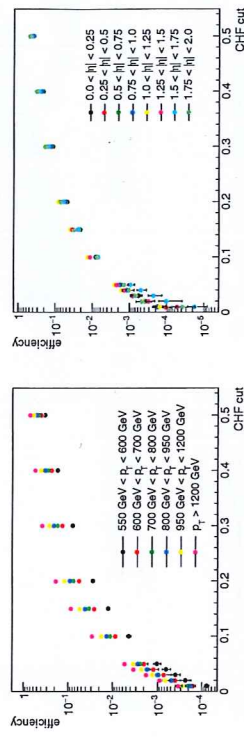


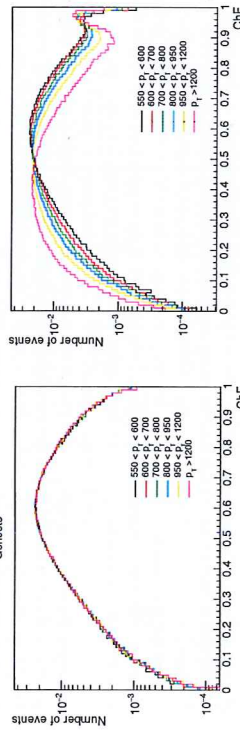
Figure 6.8: The efficiency of several CHF cuts in QCD MC, binned in p_T (left) and η (right).

A closure test is performed to validate this background prediction method, by comparing the MC truth and the 1- and 2-leg predictions in MC. The MC truth shows the yield after applying the CHF cuts on both jets. For the 1-leg prediction the CHF cut is applied on one jet and the event is then weighted by applying the measured p_T - and η -dependent efficiency for the other jet. For the 2-leg prediction, the efficiencies are applied for both jets, and no CHF cut is applied directly.

As a first check the closure test was also performed at the generator level, using the GenJets, which are reconstructed from the generator level particles. This comparison is done in exclusive bins in (CHF_{jet1}, CHF_{jet2}) , as illustrated in Figure 6.10. From Figure 6.11 one can see that there is a good agreement

*unclear
integrated over
the other
variable?
variable?*

*T_{ggf}
A lot of the method fit
using simulation and fit
(underlined below)*

Figure 6.9: The CHF per bins of p_T for generator level (left) and reconstructed (right) jets.

- 1 between MC truth, 1-, and 2-leg predictions. This shows that there are no relevant physics correlations
- 2 between the 2 jets, an essential prerequisite for this background prediction to work well. The p_T and η binning seems adequate as well.
- 3

pHWW

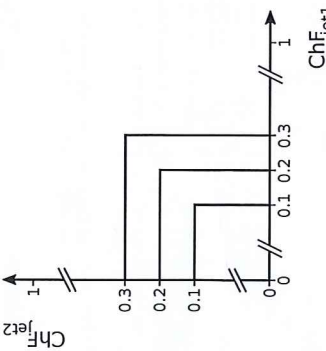
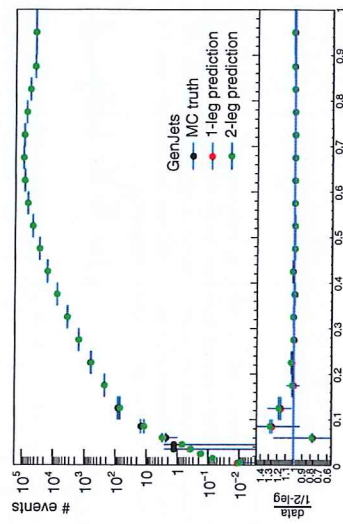


Figure 6.10: Illustration of the exclusive bins in the leading and subleading jet CHF, used for the closure test and the data vs. prediction comparisons.

- Next, the closure test is performed with reconstructed jets, as shown in the left plot of Figure 6.12, using the exclusive binning. For the MC truth, the CHF cut is applied on the 2 leading jets of the standard jet collection, as well as the 2 leading jets of the jet collection created when using the second vertex as primary vertex. This extra cut is a part of the signal region event selection described earlier, designed to remove events where the wrong primary vertex was chosen and the charged fraction of the jets is removed by CHFS. However, there is still a small discrepancy between the MC truth and the prediction at the tightest CHF cuts. This is mainly due to a very small number of events where the wrong vertex was chosen, but where the correct one is not the second one.

The closure test on MC is also performed in inclusive bins, as used in the signal region event selection, by applying the same cut on the CHF of both jets. This is shown in the right plot of Figure 6.12, with the applied CHF cut on the x-axis. For the MC truth, the statistical uncertainty is determined per HT-binned QCD sample, using asymmetric vertical bars with correct coverage for event counts with Poisson variates when less than 10 events remain, and the square root of the remaining number of events otherwise. In this way, the statistical uncertainty correctly reflects the contribution of HT bins with few or no events left. The total statistical uncertainty is then calculated by multiplying the uncertainty per HT bin by the corresponding weight for this HT bin, and adding them quadratically. The systematic uncertainty on the background prediction is then defined as the difference between the MC truth and the prediction, unless

Figure 6.9: The CHF per bins of p_T for generator level (left) and reconstructed (right) jets.

- 1 it is smaller than the statistical uncertainty on the MC truth. In that case, the uncertainty on the MC truth
- 2 is taken as systematic uncertainty.

for most out values, the statistical uncertainty dominates making the MC sample size.

scaled to what bins?

difficult to read
is this a bit weird?

Figure 6.11: Closure test using GenJets.

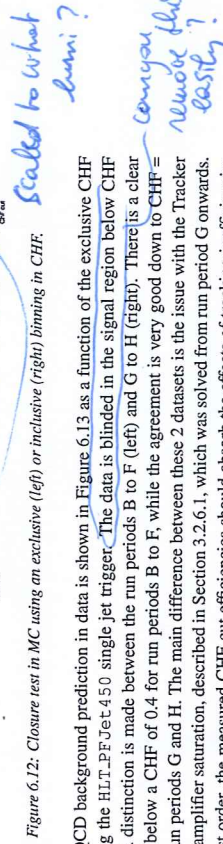


Figure 6.11: Closure test in MC using an exclusive (left) or inclusive (right) binning in CHF.

- The QCD background prediction in data is shown in Figure 6.13 as a function of the exclusive CHF bins, using the HLT_PFjet450 single jet trigger. The data is blinded in the signal region below CHF = 0.05. A distinction is made between the run periods B to F (left) and G to H (right). There is a clear deviation below a CHF of 0.4 for run periods B to F, while the agreement is very good down to CHF = 0.05 for run periods G and H. The main difference between these 2 datasets is the issue with the Tracker APV pre-amplifier saturation, described in Section 3.2.6.1, which was solved from run period G onwards. To first order, the measured CHF cut efficiencies should absorb the effects of tracking inefficiencies caused by the APV pre-amplifier saturation problem. However, this effect is also reflected in the distribution of the number of vertices. As is shown in Figure 6.14, a subtle effect causes the data and the prediction from data to disagree in the distribution of the number of vertices for run periods B to F, while a good agreement is obtained for run periods G to H. As there are not enough data to derive the CHF efficiencies reliably in bins of number of vertices as well as p_T and η , a recovery of the data in this way is not possible. A reweighting was also performed, using a fit to the ratio of data divided by the 2-leg prediction per CHF bin. Figure 6.15 shows the data versus data prediction comparison in run period E, applying the reweighting based on the number of vertices in the event, per CHF bin, and a clear improvement can be observed for the 2-leg prediction. In contrast, the 1-leg prediction has not been reweighted and still shows the original disagreement. This reweighting can however not be used in the signal region, where very few

closed hadron count
stat. uncorr
from off-tracks
are negligible

Figure 6.12: Closure test in MC using an exclusive (left) or inclusive (right) binning in CHF.

- The QCD background prediction in data is shown in Figure 6.13 as a function of the exclusive CHF bins, using the HLT_PFjet450 single jet trigger. The data is blinded in the signal region below CHF = 0.05. A distinction is made between the run periods B to F (left) and G to H (right). There is a clear deviation below a CHF of 0.4 for run periods B to F, while the agreement is very good down to CHF = 0.05 for run periods G and H. The main difference between these 2 datasets is the issue with the Tracker APV pre-amplifier saturation, described in Section 3.2.6.1, which was solved from run period G onwards. To first order, the measured CHF cut efficiencies should absorb the effects of tracking inefficiencies caused by the APV pre-amplifier saturation problem. However, this effect is also reflected in the distribution of the number of vertices. As is shown in Figure 6.14, a subtle effect causes the data and the prediction from data to disagree in the distribution of the number of vertices for run periods B to F, while a good agreement is obtained for run periods G to H. As there are not enough data to derive the CHF efficiencies reliably in bins of number of vertices as well as p_T and η , a recovery of the data in this way is not possible. A reweighting was also performed, using a fit to the ratio of data divided by the 2-leg prediction per CHF bin. Figure 6.15 shows the data versus data prediction comparison in run period E, applying the reweighting based on the number of vertices in the event, per CHF bin, and a clear improvement can be observed for the 2-leg prediction. In contrast, the 1-leg prediction has not been reweighted and still shows the original disagreement. This reweighting can however not be used in the signal region, where very few

- The QCD background prediction in data is shown in Figure 6.13 as a function of the exclusive CHF bins, using the HLT_PFjet450 single jet trigger. The data is blinded in the signal region below CHF = 0.05. A distinction is made between the run periods B to F (left) and G to H (right). There is a clear deviation below a CHF of 0.4 for run periods B to F, while the agreement is very good down to CHF = 0.05 for run periods G and H. The main difference between these 2 datasets is the issue with the Tracker APV pre-amplifier saturation, described in Section 3.2.6.1, which was solved from run period G onwards. To first order, the measured CHF cut efficiencies should absorb the effects of tracking inefficiencies caused by the APV pre-amplifier saturation problem. However, this effect is also reflected in the distribution of the number of vertices. As is shown in Figure 6.14, a subtle effect causes the data and the prediction from data to disagree in the distribution of the number of vertices for run periods B to F, while a good agreement is obtained for run periods G to H. As there are not enough data to derive the CHF efficiencies reliably in bins of number of vertices as well as p_T and η , a recovery of the data in this way is not possible. A reweighting was also performed, using a fit to the ratio of data divided by the 2-leg prediction per CHF bin. Figure 6.15 shows the data versus data prediction comparison in run period E, applying the reweighting based on the number of vertices in the event, per CHF bin, and a clear improvement can be observed for the 2-leg prediction. In contrast, the 1-leg prediction has not been reweighted and still shows the original disagreement. This reweighting can however not be used in the signal region, where very few

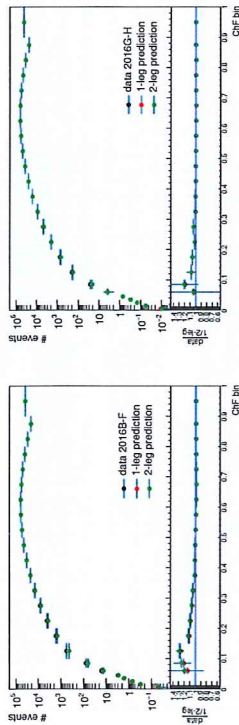


Figure 6.13: The 1- and 2-leg predictions from data, as well as the data above $\text{CHF} = 0.2$, as a function of the exclusive CHF bins, for run period E, and G-H (right).

events remain. As a result, the analysis is performed with run periods G and H only, corresponding to an integrated luminosity of 16.1 fb^{-1} .

May repeat how much above BF was,

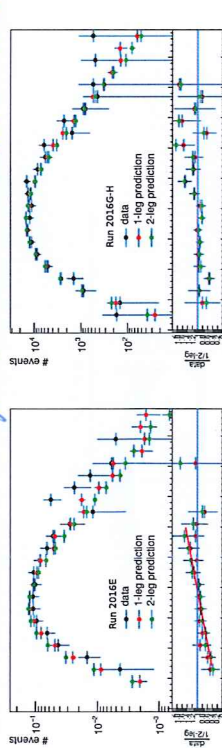


Figure 6.14: The distribution of the number of vertices for data, 1-leg, and 2-leg prediction using data from run period E (left) and run periods G-H (right).

6.5 Systematic uncertainties

For the signal prediction, systematic uncertainties are included for the luminosity, the jet energy corrections, and the trigger inefficiency at 550 GeV due to the turn-on. The systematic uncertainty for the luminosity amounts to 2.5% . The systematic uncertainty coming from the jet energy corrections is computed by varying the jet energy by the correction and recalculating the yield after applying the selection cuts and the CHF cut. Depending on the SIMP mass and the CHF cut, this uncertainty varies between 0.4% and 3.9% . A systematic uncertainty is also included to take into account the trigger inefficiency at 550 GeV due to the turn-on. This is done by taking a 100% uncertainty on the efficiency, which gives a 2% systematic uncertainty for the signal. This method does not take into account the fact that the turn-on was determined for one jet only and the inefficiency is strongly reduced when two jets with a similar p_T are present in the event. However, some signal events have one of the two jets with $\text{EMF} = 0$. In this case the jet which does not contain electromagnetic energy would not fire the single jet trigger and these events become single jet events from the trigger point of view. The 2% uncertainty is therefore conservative as it represents the worst case scenario. The photon and conversion veto was found to be 100% efficient on the signal, and as a result this systematic uncertainty is negligible. The effect of pileup was considered to be negligible as well, as the distribution of the number of vertices is very similar for the data and SIMP samples. As an example the data is compared to the SIMP sample with $m_\chi = 1000 \text{ GeV}$ in Figure 6.16, which shows that there is a good agreement in the bulk of the distribution with some deviations for a high *pileup* *but not with* *few events with*

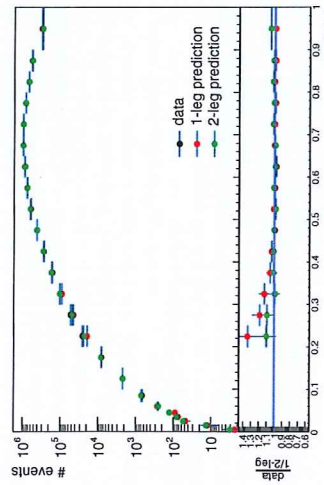


Figure 6.15: The 1- and 2-leg predictions from data, as well as the data above $\text{CHF} = 0.2$, as a function of the exclusive CHF bins for run period E, reweighting the 2-leg prediction to data based on the number of vertices in the event, per CHF bin.

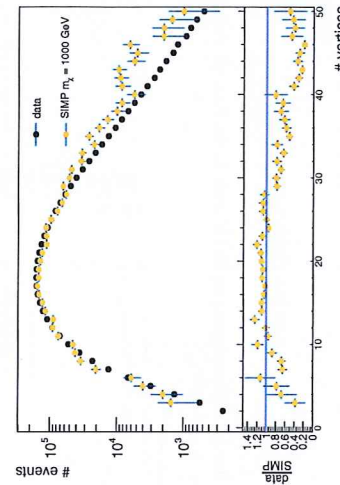


Figure 6.16: The distribution of the number of vertices in data compared to the SIMP signal with $m_\chi = 1000 \text{ GeV}$.

As mentioned in Section 6.4, the main systematic uncertainty on the background prediction is obtained from the closure test in MC, by taking the difference between the MC truth and the prediction, unless it is smaller than the statistical uncertainty on the MC truth, in which case the uncertainty on the MC truth is taken as systematic uncertainty. This uncertainty varies between 4% and 34.6% , depending on the CHF cut. As for the signal, the trigger inefficiency due to the turn-on at 550 GeV is also taken into account, yielding an additional 2% systematic uncertainty.

also for the background write Zhao!

Table 6.3 shows the number of predicted and observed events, per considered CHF cut. The prediction is done using the 1-leg data prediction, as this provides slightly smaller uncertainties due to the larger number of events that are selected to perform the prediction. The statistical uncertainty, as well as the systematic uncertainty from the closure test described in Section 6.5, are given.

6.6 Results

2-leg, me?

→ to the final signal selection

- A cut of $\text{CHF} < 0.05$ is chosen, to reject most of the QCD background. The background is then reduced to the level of about one event, and a large uncertainty does not have big consequences. Moreover,
- the uncertainty from the closure test is reduced when taking into account the smaller statistical uncertainty on the number of background events during the limit calculation. In addition, the expected sensitivity does not improve significantly at tighter CHF cuts, and the closure tests becomes statistically limited.
- The dominating uncertainty then comes from the closure test, and amounts to 250% in this case.

CHF cut	data prediction	QCD MC			SIMP signal [m_χ]	
		prediction	observed		1 GeV	1000 GeV
0.2	902 ± 5 (stat.) ± 38 (syst.)	546.5 ± 0.6	969	634	4.9	
0.15	210 ± 2 (stat.) ± 18 (syst.)	111.1 ± 0.4	229	634	4.9	
0.1	26.9 ± 0.3 (stat.) ± 8.9 (syst.)	12.6 ± 0.2	30	634	4.9	
0.07	5.1 ± 0.1 (stat.) ± 4.4 (syst.)	2.3 ± 0.2	4	634	4.9	
0.05	1.28 ± 0.03 (stat.) ± 3.24 (syst.)	0.6 ± 0.1	0	633	4.9	
0.04	0.55 ± 0.02 (stat.) ± 2.81 (syst.)	0.24 ± 0.09	0	632	4.9	
0.03	0.22 ± 0.01 (stat.) ± 7.68 (syst.)	0.08 ± 0.07	0			

Table 6.3: Number of predicted (using the 1-leg prediction from data) and observed events for the considered cuts. The expected number of signal events is also given for the $m_\chi = 1 \text{ GeV}$ and $m_\chi = 1000 \text{ GeV}$ scenarios.

Model-independent limits are derived for a $\text{CHF} < 0.05$ cut, using the CL_s criterion [134, 135] with the LHC style test statistic in which the systematic uncertainties are modelled as nuisance parameters. This was done using the RooStat-based Combine tool, taking into account the systematic uncertainties detailed in Section 6.5, as well as the statistical uncertainties on signal and background predictions. All included systematic uncertainties are profiled with a normal prior, except for the uncertainty coming from the closure test, which is profiled with a gamma function since it arises from the limited number of remaining events. The resulting expected fiducial cross section is $\sigma_{\text{fid}}^{95\%} = \sigma \times A \times \epsilon = 0.17 \text{ fb}$. With zero observed events, the observed model-independent lower limit is found to be $\sigma_{\text{fid,obs}}^{95\%} = 0.18 \text{ fb}$.

6.7 SIMP model interpretation

Limits are also derived on the production cross section for the SIMP simplified model, using the same method as described for the model-independent limits. The expected limits on the production cross section are shown for SIMP masses between 1 and 1000 GeV in Figure 6.17, using a cut of $\text{CHF} < 0.05$. In this case, the search is sensitive to all the generated SIMP mass points, up to 1000 GeV. Figure 6.18 shows the expected and observed limits when including the observation of zero events in the signal region. The expected and observed limits, and the theoretical cross section are given with respect to the generator level cuts applied in the signal sample generation, $p_T^\chi > 200 \text{ GeV}$ and $|\eta_\chi| < 2.5$. The shown theoretical cross section is also given per SIMP mass point in Table 4.3. In summary, no significant excess above the expected background is observed, and the considered SIMP simplified model is ruled out for SIMP masses up to 1000 GeV.

do you explain
this detail
more
in the way?
cheaper?
This method
is significantly
different.
What's the
difference?

do you explain
this detail
more
in the way?
cheaper?
This method
is significantly
different.
What's the
difference?

This detail
more
in the way?
cheaper?
This method
is significantly
different.
What's the
difference?

6.7 SIMP model interpretation

Limits are also derived on the production cross section for the SIMP simplified model, using the same method as described for the model-independent limits. The expected limits on the production cross section are shown for SIMP masses between 1 and 1000 GeV in Figure 6.17, using a cut of $\text{CHF} < 0.05$. In this case, the search is sensitive to all the generated SIMP mass points, up to 1000 GeV. Figure 6.18 shows the expected and observed limits when including the observation of zero events in the signal region. The expected and observed limits, and the theoretical cross section are given with respect to the generator level cuts applied in the signal sample generation, $p_T^\chi > 200 \text{ GeV}$ and $|\eta_\chi| < 2.5$. The shown theoretical cross section is also given per SIMP mass point in Table 4.3. In summary, no significant excess above the expected background is observed, and the considered SIMP simplified model is ruled out for SIMP masses up to 1000 GeV.

You could add in the explanation why
you called add the hypotheses lead to a better
higher mass hypothesis
limit ; it may be a question coming up.

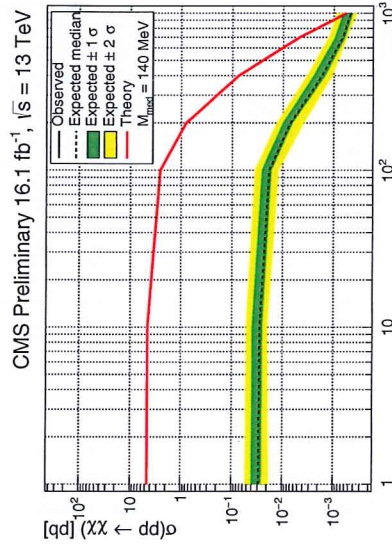


Figure 6.17: The expected limits on the production cross section, obtained without looking in the signal region, for SIMP masses between 1 and 1000 GeV, with 1 σ and 2 σ bands is shown, as well as the theoretical prediction (red), with respect to the generator level cuts ($p_T^\chi > 200 \text{ GeV}$ and $|\eta_\chi| < 2.5$).

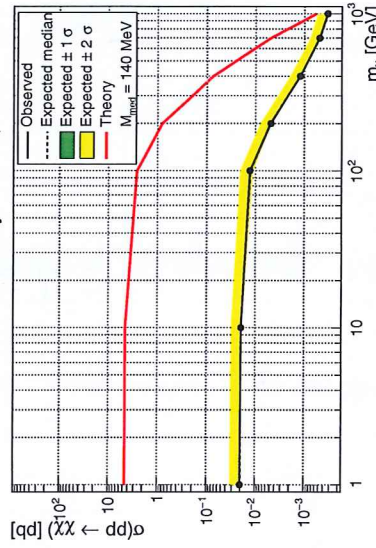


Figure 6.18: The expected and observed limits on the production cross section for SIMP masses between 1 and 1000 GeV, with 1 σ and 2 σ bands is shown, as well as the theoretical prediction (red), with respect to the generator level cuts ($p_T^\chi > 200 \text{ GeV}$ and $|\eta_\chi| < 2.5$).

do you explain
this detail
more
in the way?
cheaper?
This method
is significantly
different.
What's the
difference?

do you explain
this detail
more
in the way?
cheaper?
This method
is significantly
different.
What's the
difference?

do you explain
this detail
more
in the way?
cheaper?
This method
is significantly
different.
What's the
difference?

Toel in OPL { Ba
, Me

joeri.benharts36@gmail.com

lennart.frijnder@icloud.com